J Therm Anal Calorim (2012) 107:265–269
DOI 10.1007/s10973-011-1595-5

Thermokinetic study on the phase evolution of mechanically alloyed Ni–B powders

Masoud Nazarian-Samani · Ali Reza Kamali · Mahboobeh Nazarian-Samani · Roohallah Mobarra · Saber Naserifar

Received: 24 November 2010 / Accepted: 14 April 2011 / Published online: 1 May 2011

Abstract A combination of differential thermal analysis and detailed X-ray diffraction (XRD) analyses were used for the thermokinetic study of phase evolution during heating–cooling of the mechanically alloyed (MA-ed) Ni–15 wt% B. According to the results obtained, different phase transition sequences led to the formation of nanocrystalline Ni–B alloys comprising of Ni_2B + o-Ni_4B_3 and Ni_2B + m-Ni_4B_3 + B. Using the XRD studies, it was found that the Ni_2B is the most stable intermetallic compound in the Ni–B binary phase diagram, and its nanocrystalline nature retained unchanged even after annealing up to temperatures near the melting point. In addition, average enthalpy as well as activation energy of occurred reactions was calculated; the latter was estimated using two well-known Kissinger and Augis & Bennett methods.

Keywords Ni–B intermetallics · Nanostructured materials · Heat treatment · Thermal analysis · Mechanical alloying

M. Nazarian-Samani (✉) · M. Nazarian-Samani · R. Mobarra
Advanced Materials and Nanotechnology Research Center (AMNRC), Faculty of Mechanical Engineering, K.N. Toosi University of Technology (KNTU), Tehran, Iran
e-mail: Masoud.Nazarian@gmail.com

A. R. Kamali
Department of Materials Science and Metallurgy, University of Cambridge, Cambridge, UK
e-mail: ark42@cam.ac.uk

M. Nazarian-Samani
Department of Materials Science and Engineering, Semnan University, Semnan, Iran

S. Naserifar
Mork Family Department of Chemical Engineering and Materials Science, University of Southern California (USC), Los Angeles, CA, USA

Introduction

Ni–B binary phase diagram (Fig. 1) [1] shows several intermetallics of NiB, m-Ni_4B_3, o-Ni_4B_3, Ni_2B, and Ni_3B, respectively. These intermetallics have found interesting applications such as electroless coatings, thin/thick films, brazing filler metals, and master alloys due to their unique properties including low melting point compared to elemental constituents, excellent resistance against corrosion and wear, high electrical conductivity, and appropriate catalytic characteristics [2–8]. Moreover, they can be replaced for such noble metals as Ru, Ag, and Pd in certain electronic applications thanks to their desirable properties and lower price [3, 6]. Also, nickel borides have successfully been used as catalysts for hydrogen generation [9].

It was earlier reported that Ni–B intermetallics such as Ni_3B, Ni_2B, and o-Ni_4B_3 can be produced by an appropriate combination of MA and heat treatment [2], and it was observed that MA of Ni–15 wt% B powders for 10 h led to the formation of an interstitial solid solution, Ni(B), while heating of that gave rise to the following phase evolution:

$$\mathrm{Ni(B)} \overset{350\,^{\circ}\mathrm{C}}{\longrightarrow} \mathrm{Ni(B)} + \mathrm{Ni_3B} \overset{700\,^{\circ}\mathrm{C}}{\longrightarrow} \mathrm{Ni_3B} + \mathrm{Ni_2B} \qquad (1)$$

This article deals with the study of phase evolutions of 10 h MA-ed Ni–15 wt% B powders at higher temperatures.

Experimental procedure

A powder mixture of Ni (99.9 wt% purity, 10 μm) and B (99.9 wt% purity, 3 μm) corresponding to the composition Ni–15wt% B was MA-ed in a WC vial using WC milling balls at a powder: ball mass ratio of 1:10. The vial was filled with high purity argon and sealed with a flexible O-ring to minimize oxidation during milling. The experiments were

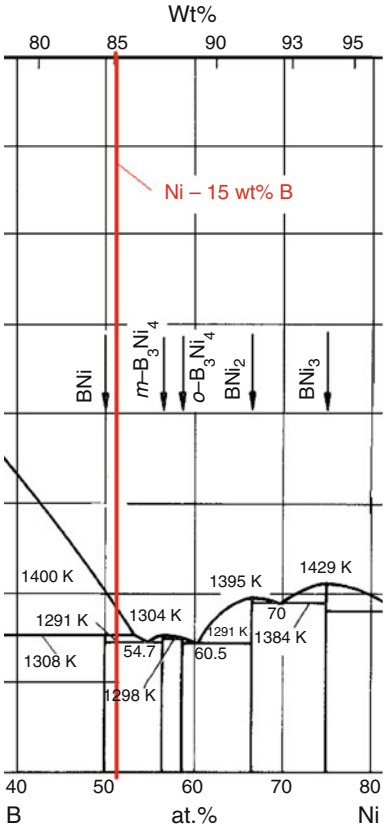

Fig. 1 Selected part of Ni–B binary phase diagram [1]

carried out in a hexane medium using a Fritsch P6 planetary ball mill at a constant speed of 300 rpm for 10 h. Thereafter, the powders were held in intermediate temperatures for removing the hexane from the compound. Details of the MA process have been published elsewhere [2]. The MA-ed powders were annealed in a tube furnace under a high purity argon atmosphere at 1030 and 1050 °C for 1 h and at a heating rate of 10 °C min^{-1} to be subsequently cooled rapidly. In addition, a small amount of the MA-ed powder was melted at 1200 °C followed by quenching in order to determine the phases produced after melting.

The annealed specimens were analyzed in a Seifert 3003TT X-ray diffractometer with Cu Kα radiation at a slow scan rate of 0.005° s^{-1}. The crystallite size of Ni_2B intermetallic compound, as a major phase at high temperatures, was estimated from the X-ray peak broadening by means of the well-known Williamson-Hall method [10–12]. In this method, the modified Scherrer's equation can be written as follow [13, 14]:

$$B\cos\theta = \frac{0.9\lambda}{d} + e\sin\theta \tag{2}$$

$$B = \sqrt{B_{\mathrm{M}}^2 - B_{\mathrm{I}}^2} \tag{3}$$

where, B is the modified peak full width at half the maximum (FWHM) of X-ray diffraction (XRD) patterns, θ is the Bragg angle, λ is the wavelength of the X-ray used, d is the crystallite size, e is the lattice strain, B_{M} and B_{I} refer to milled and annealed powders, respectively. Thus, when Bcos θ was plotted against sin θ, a straight line was obtained with the slope as e and the intercept as 0.9 λ/d. From these, crystallite size, d, and lattice strain, e, were calculated [13]. It is worth noting that FWHM was obtained by Lorentzian curve fitting of X-ray peaks. The uncertainties in the particle sizes were estimated from the errors in the Lorentzian function, and it was found to be ±1 nm.

The structural change and phase transformation processes of the MA-ed powder upon heating was also investigated using a NETZSCH STA 409 PC/PG differential thermal analyzer under an Ar flow. About 80–100 mg of the 10 h-milled powder was subjected to differential thermal analysis (DTA) at different selected heating rates (5, 10, 15, 20, and 50 °C min^{-1}). The temperature covered in the DTA ranged from room temperature to 1200 °C. Temperature calibration was accomplished using the melting points of pure silver and gold standards.

The effective activation energy of different transitions (E_{c}) was determined using the Kissinger [15] and the Augis & Bennett (A&B) methods [16]:

$$\ln\frac{\beta}{T_p^2} = -\frac{E_{\mathrm{c}}}{RT_p} + \text{constant} \tag{4}$$

$$\ln\frac{\beta}{T_p - T_o} = -\frac{E_{\mathrm{c}}}{RT_p} + \text{constant} \tag{5}$$

where β is heating rate, R is gas constant, and T_{o} and T_p are initial and specific temperatures, respectively.

Results and discussions

Thermal phase evolution

Figure 2 presents the DTA analysis of 10 h MA-ed Ni–15 wt% B powders heated up to 1200 °C at different heating rates. Clearly, the curves comprise two exothermic peaks followed by two endothermic ones. It was already shown that the 10 h MA-ed Ni–15 wt% B powders comprise of a saturated solid solution of Ni(B). Also it was observed that the first exothermic peak is related to the formation of Ni_3B from Ni(B) [2]. The identity of other peaks can be verified by XRD measurement. For this purpose, the MA-ed powders were annealed at different temperatures and the annealed samples underwent XRD measurements, as shown in Fig. 3.

Identification of the second peak

The second peak appeared at about 700–717 °C, depending on the heating rate (Fig. 2), can be related to the formation of Ni_2B from Ni_3B detected by XRD pattern taken from the sample annealed at 800 °C, which is in agreement with the previous study [2]. It is worthy being noted that there are no strong B–B bonds in Ni_3B [9], while existence of these bonds has been proved in compounds with higher ratio of boron to nickel contents [17]. Therefore, the transformation of Ni_3B to Ni_2B is accompanied by the release of heat.

Identification of third peak

It is clear from Fig. 3 that heating the powder up to about 1030 °C causes the remaining Ni_3B peaks to vanish but *o*-Ni_4B_3 peaks to appear. Therefore, the third peak which appears at 1028–1042 °C (Fig. 2) can be attributed to the formation of *o*-Ni_4B_3. As it can be seen in Fig. 2, the third peak is an endothermic peak, while it is well known that nickel borides are formed during exothermic reactions with enthalpies of formation typically between −300 and −50 kJ mol^{-1} [18]. Also, formation of *o*-Ni_4B_3 with a high ratio of boron/nickel should be accompanied with energy release. The endothermic nature of third peak may be explained considering partial melting of the heat-treated sample. The third peak at 1028–1042 °C can be attributed to the occurrence of following reaction sequence:

$$Ni_2B + Ni_3B \xrightarrow{\text{Heating to } 1028-1042\,^{\circ}C} Ni_2B + L_1 \xrightarrow{\text{Cooling to } 25\,^{\circ}C} Ni_2B + o\text{-}Ni_4B_3 \quad (6)$$

where L_1 is a Ni–B liquid-phase eutectic. According to Fig. 3, increasing the annealing temperature to 1050 °C had no considerable effect on the product unless a slight increase in *o*-Ni_4B_3 peaks intensity compared to those of Ni_2B.

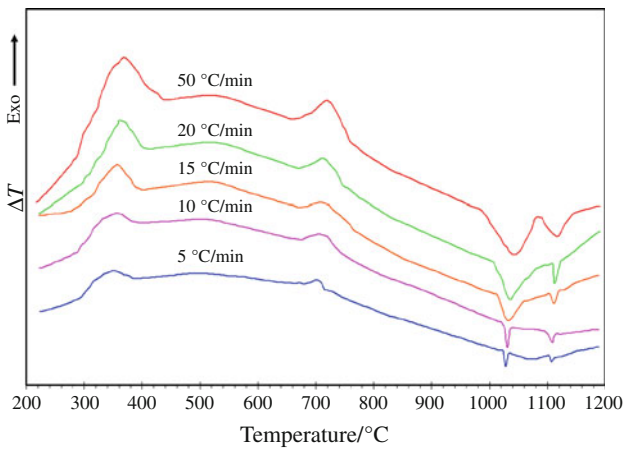

Fig. 2 Non-isothermal DTA curves of Ni–15 wt% B alloy at various heating rates

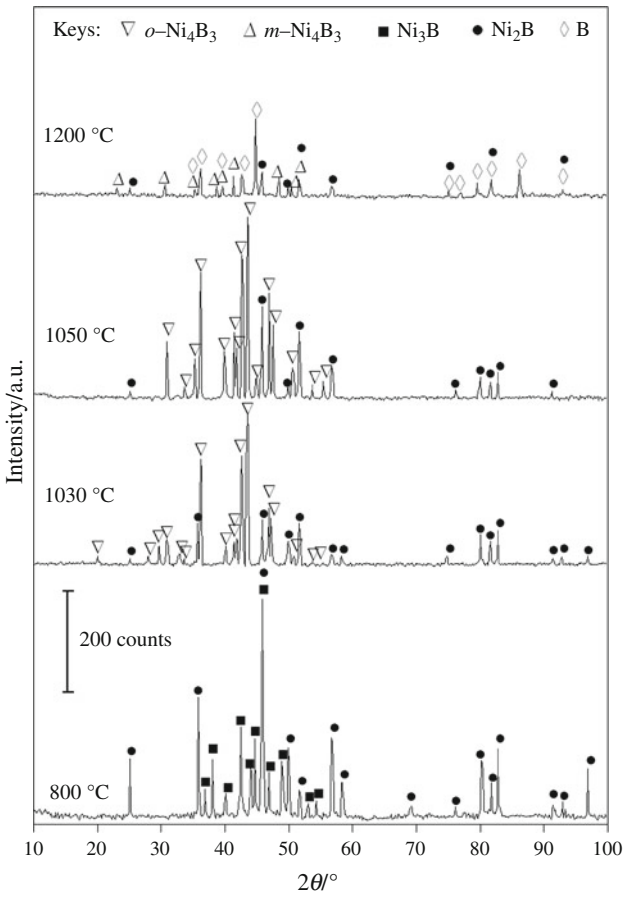

Fig. 3 XRD patterns of heat treated powders at different temperatures

Identification of forth peak

It can be recognized from Fig. 3 that the *o*-Ni_4B_3 peaks have vanished and those of *m*-Ni_4B_3 and B phases have appeared upon heating the sample to 1200 °C followed by its cooling to room temperature, where a complete melting of the material was achieved. It should be noticed that *m*-Ni_4B_3 is thermodynamically stable at the chemical composition of the alloy (Fig. 1). Formation of this phase could be an indication of equilibrium thermodynamic approach of the transformation at higher temperatures. Similar to the case of third peak, the fourth endothermic peak occurred at

Table 1 Variations in crystallite size of Ni_2B intermetallic compound at different temperatures

Temperature/°C	800	1030	1050
Crystallite size/nm	49	65	72

Table 2 Enthalpies estimated from integrated areas of DTA curves and corresponding peak temperatures

Heating rate/°C min^{-1}	First peak		Second peak		Third peak		Fourth peak	
	T_p/°C	ΔH/kJ mol^{-1}	T_p/°C	ΔH/kJ mol^{-1}	T_p/°C	ΔH/kJ mol^{-1}	T_p/°C	ΔH/kJ mol^{-1}
5	350.96	−93.65	700.85	−64.42	1028.45	58.28	1106.96	28.10
10	355.43	−112.91	704.36	−71.18	1031.14	64.62	1108.44	33.32
15	357.04	−128.12	708.12	−87.36	1033.85	91.75	1111.46	51.83
20	360.26	−141.62	711.35	−105.79	1035.71	113.93	1112.85	62.17
50	369.93	−165.77	717.17	−131.73	1042.62	125.78	1117.85	87.43

Table 3 Activation energies of third and fourth peaks calculated based on Kissinger and A&B plots

Calculation method	Third peak		Fourth peak	
	E_C/kJ mol^{-1}	|R|	E_C/kJ mol^{-1}	|R|
Kissinger	2212.88	0.9799	3133.70	0.9713
A&B	2220.53	0.9800	3141.59	0.9714

the temperature of 1107–1118 °C can be attributed to the occurrence of following reaction sequence:

$$\mathrm{Ni_2B} + \mathrm{Ni_3B} \overset{\text{Heating to } 1028-1042\,^\circ\mathrm{C}}{\longrightarrow} \mathrm{Ni_2B} + \mathrm{L_1} \overset{\text{Heating to } 1107-1118\,^\circ\mathrm{C}}{\longrightarrow} \mathrm{L_2} \overset{\text{Cooling to } 25\,^\circ\mathrm{C}}{\longrightarrow} \mathrm{Ni_2B} + m\text{-}\mathrm{Ni_4B_3} + \mathrm{B} \quad (7)$$

where L_2 is a Ni–B liquid phase with the composition of Ni–15 wt% B. Formation of Ni_2B + m-Ni_4B_3 + B instead of NiB + m-Ni_4B_3 (Fig. 1) upon cooling of Ni–15 wt% B melt can be attributed to the non-equilibrium cooling rate of alloy.

Based on the binary phase diagram of Ni–B (Fig. 1), at composition of Ni–15 wt% B the stable phases at room temperature have to be NiB and m-Ni_4B_3. As it can be seen from Eqs. 6 and 7, the room temperature phases produced upon cooling of 10 h MA-ed Ni–15 wt% B powders annealed at 1028–1042 °C and 1107–1118 °C were Ni_2B + o-Ni_4B_3 and Ni_2B + m-Ni_4B_3 + B, respectively. The lack of the formation of equilibrium phases during the heating of the material mainly can be attributed to the non-equilibrium condition of the MA-ed powders. However, as it was mentioned, the product of the reactions approaches to more thermodynamically stable phases upon thermal progress of transformations. Obtained results interestingly recommend a new approach for producing the multiphase Ni–B intermetallic alloys which cannot be produced by near-equilibrium processes.

As it can be found from Eq. 7, Ni_2B has been stable since its formation at about 700 °C up to more than 1100 °C. It should be considered that the structure-type of Ni_2B is that of $CuAl_2$-θ, which a distorted fluorite atomic arrangement with alternate Ni layers has rotated by 45° relative to one another [19]. It is worthy to notice that if the ratio of boron radius to a transition metal radius in $CuAl_2$ structures falls in 0.62–1.01, the corresponding compounds are thermally stable [19, 20]. Therefore, thermal stability of Ni_2B with a ratio of 0.738 [20] can be explained. Variations in crystallite size of Ni_2B intermetallic compound at different temperatures can be found in Table 1. According to this Table, Ni_2B has kept its fine crystallite size even after heating the powders to a temperature as high as 1050 °C.

Thermokinetic evaluations

It can be deduced from Fig. 2 that the critical temperatures increase with increasing the heating rate. Table 2 lists maximum peak temperatures (T_p) as a function of heating rate for the four transformations displayed in Fig. 2. The Table also presents the average values for the enthalpy of occurred reactions, measured as the area directly under the peak.

The activation energy of the third and fourth transformations taking place in this system can be calculated by using the peak temperatures presented in Table 2 and Eqs. 4 and 5. The activation energies, presented in Table 3, were calculated based on the slopes of the plotted data. These values calculated by both methods were found to be in excellent agreement.

Conclusions

Phase evolution in the 10 h MA-ed Ni–15 wt% B powders at the temperature range of 800–1200 °C was found to be as follows:

$$\mathrm{Ni_2B} + \mathrm{Ni_3B} \overset{\text{Heating to } 1028-1042\,^\circ\mathrm{C}}{\longrightarrow} \mathrm{Ni_2B} + \mathrm{L_1} \overset{\text{Heating to } 1107-1118\,^\circ\mathrm{C}}{\longrightarrow} \mathrm{L_2}$$

where the activation energy of reactions corresponding to the formation of Ni_2B + L_1 and L_2 was found to be around 2200 and 3100 kJ mol^{-1}, respectively. Production of non-equilibrium crystalline phases of Ni_2B + m-Ni_4B_3 + B upon heating–cooling of 10 h MA-ed Ni–15 wt% B

powders can introduce a new approach for producing multiphase nanocrystalline alloys in the Ni–B system.

References

1. Predel B. B-Ni (Boron-Nickel). In: Madelung O, editor. SpringerMaterials—the Landolt-Börnstein Database (http://www.springermaterials.com). doi: 10.1007/10040476-370.
2. Nazarian-Samani M, Kamali AR, Mobarra R, Nazarian-Samani M. Phase transformations of Ni–15wt% B powders during mechanical alloying and annealing. Mater Lett. 2010;64:309–12.
3. Paustovskii AV, Rud' BM, Tel'nikov EY, Vlasenko AI, Shelud'ko VE, Smirnov AB. Laser treatment of thick films based on powder composites of nickel boride. Powder Metall Met Ceram. 2002;41:119–22.
4. Li Q, Zhang D, Lei T, Chen C, Chen W. Comparison of laser-clad and furnace-melted Ni-based alloy microstructures. Surf Coat Technol. 2001;137:122–35.
5. Riddle YW, Bailer TO. Friction and wear reduction via a Ni-B electroless bath coating for metal alloys. JOM. 2005;57:40–5.
6. Sankara Narayanan TSN, Seshadri SK. Formation and characterization of borohydride reduced electroless nickel deposits. J Alloys Compd. 2004;365:197–205.
7. Feng X, Bai YJ, Lü B, Zhao YR, Yang J, Chi JR. Synthesis of nanocrystalline Ni_2B via a solvo-thermal route. Inorg Chem Commun. 2004;7:189–91.
8. Azhazha VM, Semenenko VE, Pilipenko NN. Synthesis of nanocrystalline Ni_2B via a solvo-thermal route. Powder Metall Met Ceram. 2007;46:32–7.
9. Wu C, Bai Y, Wu F, Wang G. Nickel boride alloys as catalysts for successive hydrogen generation from sodium borohydride solution. Trans Nonferrous Met Soc China. 2007;17:1002–5.
10. Williamson GK, Hall WH. X-ray broadening from field aluminium and wolfram. Acta Metall. 1953;1:22–31.
11. Warren BE. X-ray diffraction. New York: Dover Publications; 1990.
12. Klug HP, Alexander LE. X-ray diffraction procedures for polycrystalline and amorphous materials. London: Wiley; 1954.
13. Suryanarayana C. Mechanical alloying and milling. New York: Marcel Dekker; 2004.
14. Nazarian-Samani M, Shokuhfar A, Kamali AR, Hadi M. Production of a nanocrystalline Ni_3Al-based alloy using mechanical alloying. J Alloys Compd. 2010;500:30–3.
15. Kissinger HE. Variation of peak temperature with heating rate in differential thermal analysis. J Res Natl Bur Stand. 1956;57:217–21.
16. Augis JE, Bennet J. Calculations of avrami parameters for heterogeneous solid state reactions using a modification of the Kissinger method. J Therm Anal. 1978;13:283–7.
17. Bratkovsky AM, Smirnov AV. The topological characteristics and electron bonding in simple and metal-metalloid systems: crystal, liquid, glass versus penrose lattice. J Non-Cryst Solids. 1990;117(118):211–4.
18. Gordienko SP. Thermodynamic characteristics of iron subgroup borides. Powder Metall Met Ceram. 2002;41:169–72.
19. Havinga EE, Damsma H. Compounds and pseudo-binary alloys with the $CuAl_2$ (C16)—type structure, III. Stability and competitive structures. J Less-Common Met. 1972;27:269–80.
20. Havinga EE, Damsma H, Hokkeling P. Compounds and pseudo-binary alloys with the $CuAl_2$(C16)—type structure, I. Preparation and X-ray results. J Less-Common Met. 1972;27:169–86.